Cancer Science
Japanese Cancer Association JCA
Open Access

Enhanced antitumor effect of anti-tissue factor antibody-conjugated epirubicin-incorporating micelles in xenograft models

Yoshiyuki Yamamoto,[1,2] Ichinosuke Hyodo,[2] Yoshikatsu Koga,[1] Ryo Tsumura,[1] Ryuta Sato,[1] Toshihumi Obonai,[1] Hirobumi Fuchigami,[1] Fumiaki Furuya,[1] Masahiro Yasunaga,[1] Mitsunori Harada,[3] Yasuki Kato,[3] Atsushi Ohtsu[4] and Yasuhiro Matsumura[1]

[1]Division of Developmental Therapeutics, Research Center for Innovative Oncology, National Cancer Center Hospital East, Kashiwa; [2]Department of Gastroenterology and Hepatology, Institute of Clinical Medicine, Graduate School of Comprehensive Human Sciences, University of Tsukuba, Tsukuba; [3]Research Division, NanoCarrier Co. Ltd., Kashiwa; [4]Exploratory Oncology Research and Clinical Trial Center, National Cancer Center, Tokyo, Japan

Key words

Antibody drug conjugate, drug delivery system, epirubicin, polymeric micelles, tissue factor

Correspondence

Yasuhiro Matsumura, Division of Developmental Therapeutics, Research Center for Innovative Oncology, National Cancer Center Hospital East, 6-5-1 Kashiwanoha, Kashiwa, Chiba 277-8577, Japan.
Tel: +81-(0)-4-7134-6857; Fax: +81-(0)-4-7134-6866;
E-mail: yhmatsum@east.ncc.go.jp

Funding Information

This work was supported by the Funding Program for World-Leading Innovative R&D on Science and Technology (FIRST Program), the National Cancer Center Research and Development Fund (26-A-14).

Received December 5, 2014; Revised February 7, 2015; Accepted February 20, 2015

Cancer Sci **106** (2015) 627–634

doi: 10.1111/cas.12645

For the creation of a successful antibody–drug conjugate (ADC), both scientific and clinical evidence has indicated that highly toxic anticancer agents (ACA) should be conjugated to a monoclonal antibody (mAb) to administer a reasonable amount of ADC to patients without compromising the affinity of the mAb. For ordinary ACA, the conjugation of a mAb to ACA-loaded micellar nanoparticles is clinically applicable. Tissue factor (TF) is often overexpressed in various cancer cells and tumor vascular endothelium. Accordingly, anti-TF-NC-6300, consisting of epirubicin-incorporating micelles (NC-6300) conjugated with the $F(ab')_2$ of anti-TF mAb was developed. The *in vitro* and *in vivo* efficacy and pharmacokinetics of anti-TF-NC-6300 were compared to NC-6300 using two human pancreatic cancer cell lines, BxPC3 (high TF expression) and SUIT2 (low TF expression), and a gastric cancer cell line, 44As3 (high TF expression). The intracellular uptake of epirubicin was faster and greater in BxPC3 cells treated with anti-TF-NC-6300, compared with NC-6300. Anti-TF-NC-6300 showed a superior antitumor activity in BxPC3 and 44As3 xenografts, compared with NC-6300, while the activities of both micelles were similar in the SUIT2 xenograft. A higher tumor accumulation of anti-TF-NC-6300 compared to NC-6300 was seen, regardless of the TF expression levels. However, anti-TF-NC-6300 appeared to be localized to the tumor cells with high TF expression. These results indicated that the enhanced antitumor effect of anti-TF-NC6300 may be independent of the tumor accumulation but may depend on the selective intratumor localization and the preferential internalization of anti-TF-NC-6300 into high TF tumor cells.

The success of T-DM1 in patients with metastatic breast cancer[1] and of brentuximab vedotin in patients with some types of lymphoma[2,3] has furthered interest in active targeting or antibody–drug conjugates (ADC) in a robust fashion. However, fewer than three anticancer agent (ACA) molecules, on average, should be conjugated to the monoclonal antibody (mAb); the affinity of the mAb is diminished if too many ACA molecules are attached to the mAb.[4] According to this principle, an unrealistic amount of ADC must be administered if the mAb are conjugated with an ordinary ACA, such as taxanes or anthracyclines. Therefore, the ADC strategy should be confined to highly toxic anticancer agents, rather than ordinary ACA. Instead, for ordinary ACA, nanoparticles should be considered as a drug delivery system (DDS) tool. Kataoka *et al.* developed ACA that incorporated micelles for the first time based on the enhanced permeability and retention (EPR) effect,[5,6] and several preclinical studies have since demonstrated the advantages of using ACA-incorporating polymeric micelles, some of which are currently under clinical evaluation.[7–15]

Tissue factor (TF), which is the primary initiator of coagulation, is now known to play important roles in tumor proliferation, invasion and metastasis.[16] TF is highly expressed on the surface of almost all human tumor cells, and alternatively spliced soluble TF is also produced by many types of tumors.[16,17] In addition, TF is recognized as a prognostic factor in various cancers.[16] Based on these data, we successfully undertook the development of a mAb against human TF, 1849 clone.[18]

To date, several polymeric micelles with an active targeting ability using tumor-specific antibodies (such as trastuzumab, 2C5 and HAb18) have been developed and have been shown to exhibit potent anticancer activity.[19–26] In the present study, we succeeded in developing anti-TF mAb-conjugated epirubicin-incorporating polymeric micelles (anti-TF-NC-6300). Here, for the first time, we report the biochemical characteristics, the results of *in vitro* and *in vivo* pharmacological studies, and the antitumor activity of anti-TF-NC6300.

Materials and Methods

Drugs. NC-6300 was prepared by NanoCarrier (Kashiwa, Japan). Epirubicin was purchased from Pfizer Japan (Tokyo, Japan).

Cell cultures and cell selection based on tissue factor expression. The human gastric cancer cell lines MKN1, MKN45 and MKN74 were purchased from the JCRB Cell Bank (Osaka, Japan). 44As3, a human signet-ring cell gastric cancer cell line, was kindly provided by Dr K. Yanagihara (National Cancer Center Hospital East, Kashiwa, Japan). The human pancreatic cancer cell lines BxPC3, Capan1, Panc1 and PSN1 were purchased from the American Type Culture Collection (Rockville, MD, USA) and SUIT2 was purchased from the JCRB Cell Bank. All cell lines were authenticated by short tandem repeat DNA profiling by the JCRB Cell Bank. The TF expression levels of various gastric and pancreatic cell lines were examined using a flow cytometry analysis.

Preparation of anti-TF-NC-6300. The 1849 antibody was prewarmed in a reaction buffer containing 125 mM sodium citrate and 100 mM lithium chloride (pH 3.5) for 30 min at 37°C, then digested with pepsin (Wako, Osaka, Japan) at a protein /enzyme ratio of 100:1 for 30 min at 37°C. The digestion was stopped by raising the pH to 7.0 using 1.5 M Tris–HCl (pH 10.0). The reaction buffer was exchanged for PBS using Amicon Ultra (Merck-Millipore, Darmstadt, Germany). 1849-F $(ab')_2$ was purified using molecular sieve chromatography with a HiLoad Superdex 16/600 Superdex 200 pg column (GE Healthcare, Uppsala, Sweden).

Anti-TF-NC-6300 was prepared based on our antibody/drug-conjugated micelle technology, with slight modification. Briefly, NC-6300 and maleimide-polyethylene glycol (PEG)-poly (glutamic acid benzyl ester) were mixed at a weight ratio of 4:1 and dissolved in methanol. The solvent was evaporated completely using a rotary evaporator *in vacuo*. The resultant polymer film was hydrated with PBS to prepare the polymeric micelles through sonication. Thiolated antibody with 2-iminothiolane was covalently conjugated to the terminal maleimide groups of the PEG at the micelle surface. The micelles were then purified from unreacted antibody using ultrafiltration. The collected micelles were reacted with cysteine to mask the residual maleimide groups. The micellar nanoparticles were applied to PD-10 desalting columns (GE Healthcare) to exchange the solvent for 10% (w/v) sucrose and then stored at −80°C prior to use. The antibody concentration of anti-TF-NC-6300 was determined using reversed phase HPLC after acid hydrolysis and one anti-TF-NC-6300 molecule appeared to contain four molecules of $F(ab')_2$ at the termini of PEG chains on the particle surface (Fig. 1a–d).

Cellular uptake and affinity analysis. A flow cytometry analysis was performed to assess the cellular affinity of various types of anti-TF antibodies, NC-6300 and anti-TF-NC-6300. Two cell lines with high TF expression levels, 44As3 and BxPC3, were used to evaluate the binding activity of anti-mouse TF mAb, anti-human TF mAb, anti-human TF $F(ab')_2$, NC-6300 and anti-TF-NC-6300.

Imaging cytometric analysis and quantification of cellular uptake of epirubicin. BxPC3 cells (high TF expression) and SUIT2 cells (low TF expression) were placed in 96-well plates at 5000 cells/well in a final volume of 100 μL and incubated for 24 h at 37°C. The medium was then removed, and anti-TF-NC-6300, NC-6300 or epirubicin was added at a suitable concentration of 2.5 μM to the wells (each drug concentration was determined in epirubicin equivalents) and incubated for 1, 3, 6, 12, 24, 36 or 48 h at 37°C. After each

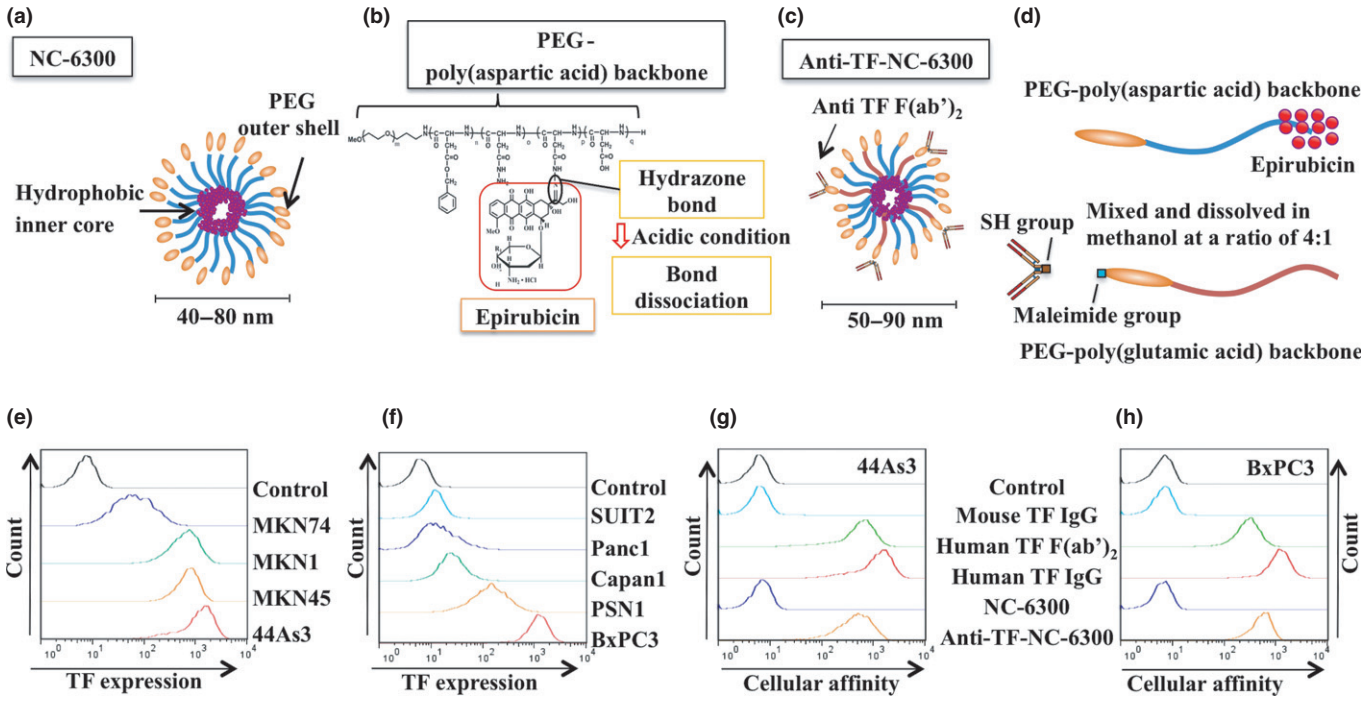

Fig. 1. Structure of NC-6300 (a). NC-6300 is comprised of epirubicin covalently bound to a polyethylene glycol (PEG)-poly (aspartic acid) block copolymer through an acid-labile hydrazone bond (b). Anti-TF-NC-6300 (c) was prepared based on our antibody/drug-conjugated micelle technology with slight modification (d). Comparative flow cytometry analysis for tissue factor (TF) expression by human gastric cancer cells (e) and pancreatic cancer cells (f). Comparative flow cytometry analysis for cellular affinity of 44As3 cells (g) and BxPC3 cells (h) to various anti-TF antibodies, NC-6300 and anti-TF-NC-6300.

incubation period, the medium was aspirated and 100 μL of 4% paraformaldehyde was added; the cells were then kept at room temperature for 10 min. After washing with PBS three times, the nuclei of the cells were stained in DAPI (×1000) for 5 min. The cells were washed with PBS three times. Images were obtained using an ArrayScan VTI Reader (Thermo Scientific, Rockford, IL, USA). Epirubicin was imaged using the TRITC XF93 filter set, and nuclei were imaged using the Hoechst XF93 filter set. The fluorescence signals from epirubicin in the cytoplasm plus membrane or nucleus were quantified using the Analysis algorithm (Compartmental Analysis V4) of Cellomics BioApplications (Thermo Scientific). The output parameters that were used consisted of the mean ring total intensity per object (cytoplasm plus membrane) and the mean circle total intensity per object (nucleus). The minimum acceptable number of cells used for the image analysis of each well was set at 300 cells.

***In vitro* real-time growth-inhibition assay.** In the *in vitro* assay, real-time cell analysis was performed using the xCELLigence system (ACEA Bioscience, San Diego, CA, USA). First, the optimal seeding concentration for the cell proliferation study of BxPC3 and SUIT2, which reached a confluent status after 120 h, was determined. Next, the optimal drug concentration was determined to monitor cell proliferation. As a result, BxPC3 and SUIT2 cells were placed in 96-well E-plates at 1000 cells/well in a final volume of 100 μL and were incubated for 24 h at 37°C. The medium was then removed, and anti-TF-NC-6300, NC-6300 and epirubicin were added at a suitable concentration of 0.05 μM in BxPC3 or 0.5 μM in SUIT2 (each drug concentration was determined in epirubicin equivalents). The proliferation of each cell line was monitored by xCELLigence system software. The quantification of proliferating cells was determined as the cell index based on the detected cell-electrode impedance in each well. The cell index was normalized at the time point of adding drugs and acquired every 60 min for 120 h.

***In vivo* antitumor activity.** Female BALB/c nu/nu mice were purchased from Japan SLC (Shizuoka, Japan) and CLEA Japan (Tokyo, Japan). Mice that were 5–6 weeks' old were subcutaneously inoculated with 5×10^5 44As3 cells (high TF expression), 1×10^7 BxPC3 cells (high TF expression) or 3×10^6 SUIT2 cells (low TF expression) in the flank region. When the tumor volume reached 150 mm^3 (44As3), 200 mm^3 (BxPC3) or 250 mm^3 (SUIT2), the mice were randomly divided into four test groups consisting of five mice each (day 0). The test drugs were administered intravenously on days 0, 7 and 14 via the tail vein. The test groups received anti-TF-NC-6300 (10 mg/kg, epirubicin equivalent), NC-6300 (10 mg/kg, epirubicin equivalent) or epirubicin (10 mg/kg). The length (a) and width (b) of the tumor masses were measured twice each week until day 28, and the tumor volume (TV) was calculated using the following equation: $TV = (a \times b^2)/2$. For humane reasons, the animals in which the tumor volume exceeded 2000 mm^3 were sacrificed. The body weight of each mouse was also measured until day 28. All the animal procedures were performed in compliance with the Guidelines for the Care and Use of Experimental Animals established by the Committee for Animal Experimentation of the National Cancer Center; these guidelines meet the ethical standards required by law and also comply with the guidelines for the use of experimental animals in Japan.

Pharmacokinetic analysis. When the average tumor volume reached 500 mm^3 after the inoculation of BxPC3 cells and SUIT2 cells, the mice were injected with anti-TF-NC-6300 (10 mg/kg) or NC-6300 (10 mg/kg) intravenously. Under general anesthesia, blood was collected via cardiac puncture, and tumors, livers and kidneys were excised at 0.17, 1, 6, 24 and 120 h, respectively, after the drug administration. In the case of mice bearing SUIT2 tumor, only tumor tissues were excised. The pharmacokinetic analysis was conducted using three mice for each time-point. The concentrations of both the free epirubicin (i.e. that released *in vivo* from anti-TF-NC-6300/NC-6300) and total epirubicin (i.e. that released from anti-TF-NC-6300/NC-6300 plus the remainder of anti-TF-NC-6300/NC-6300) were determined using high-performance liquid chromatography (HPLC) (RF-20AXS; Shimadzu Corporation, Kyoto, Japan) as described previously.[13]

Distribution of anti-TF-NC-6300 in tumor tissues. The mice bearing BxPC3 or SUIT2 tumor were injected with Alexa Fluor 647-labeled anti-TF-NC-6300 (50 mg/kg) (Molecular Probes, Life Technologies, OR, USA) intravenously. Under general anesthesia, tumors were excised at 24 h after the drug administration. The samples were embedded in an OCT compound (Sakura Finetechnochemical, Tokyo, Japan) and quickly frozen in liquid nitrogen. Six-micrometer-thick frozen sections were prepared and fixed in 4% paraformaldehyde in PBS. After blocking, sections were incubated for 1 h at room temperature with goat anti-mouse CD31 antibody for endothelial cells (R&D Systems, Minneapolis, MN, USA) at 1:100 dilution. The sections were then incubated with donkey anti-goat polyclonal antibody as a secondary antibody at 1:500 dilution. Nuclei were counterstained with 4′,6-diamidino-2-phenylindole at 1:1000 dilution. For observation of the fluorescence of Alexa Fluor 647-labeled anti TF-NC-6300, the frozen sections were examined under a fluorescence microscope, BIOREVO BZ9000 (Keyence, Osaka, Japan).

Statistical analysis. Data were expressed as the mean ± SD and were analyzed using Student's t-test when groups showed equal variances (F-test) or the Welch test when they showed unequal variances (F-test) in the *in vitro* real-time growth-inhibition assay and the quantification assay for the cellular uptake of epirubicin. A repeated-measures ANOVA was used to evaluate the *in vivo* antitumor effects of the drugs and the changes in the body weight of each treatment group. The level of significance for all the tests was set at $P < 0.05$. All the statistical tests were two-sided. These analyses were conducted using SPSS, version 19.0 (SPSS, Chicago, IL, USA).

Results

Binding of anti-TF-NC-6300 to cancer cell lines with high tissue factor expression levels. The gastric cancer cell line 44As3 and the pancreatic cancer cell line BxPC3 showed high TF expression and were, therefore, used to evaluate the binding activities of the anti-TF-NC-6300 and anti-TF antibodies (Fig. 1e,f). The TF binding affinity of anti-TF-NC-6300 was two orders of magnitude higher than that of NC-6300 in the 44As3 and BxPC3 cells. In addition, the TF binding affinity of anti-TF-NC-6300 was almost equivalent to that of anti-human TF F $(ab')_2$ in both cell lines (Fig. 1g,h).

Cellular uptake of epirubicin following exposure to conventional epirubicin, NC-6300 and anti-TF-NC-6300. Free epirubicin showed the fastest internalization into the cytoplasm and then the nucleus, compared with anti-TF-NC-6300 and NC-6300, in both cell lines (Fig. 2a,b). Between the anti-TF-NC-6300 and NC-6300, the anti-TF-NC-6300 was internalized sooner and more efficiently into the cytoplasm and nucleus in the BxPC3 cells (high TF expression) (Fig. 2a).

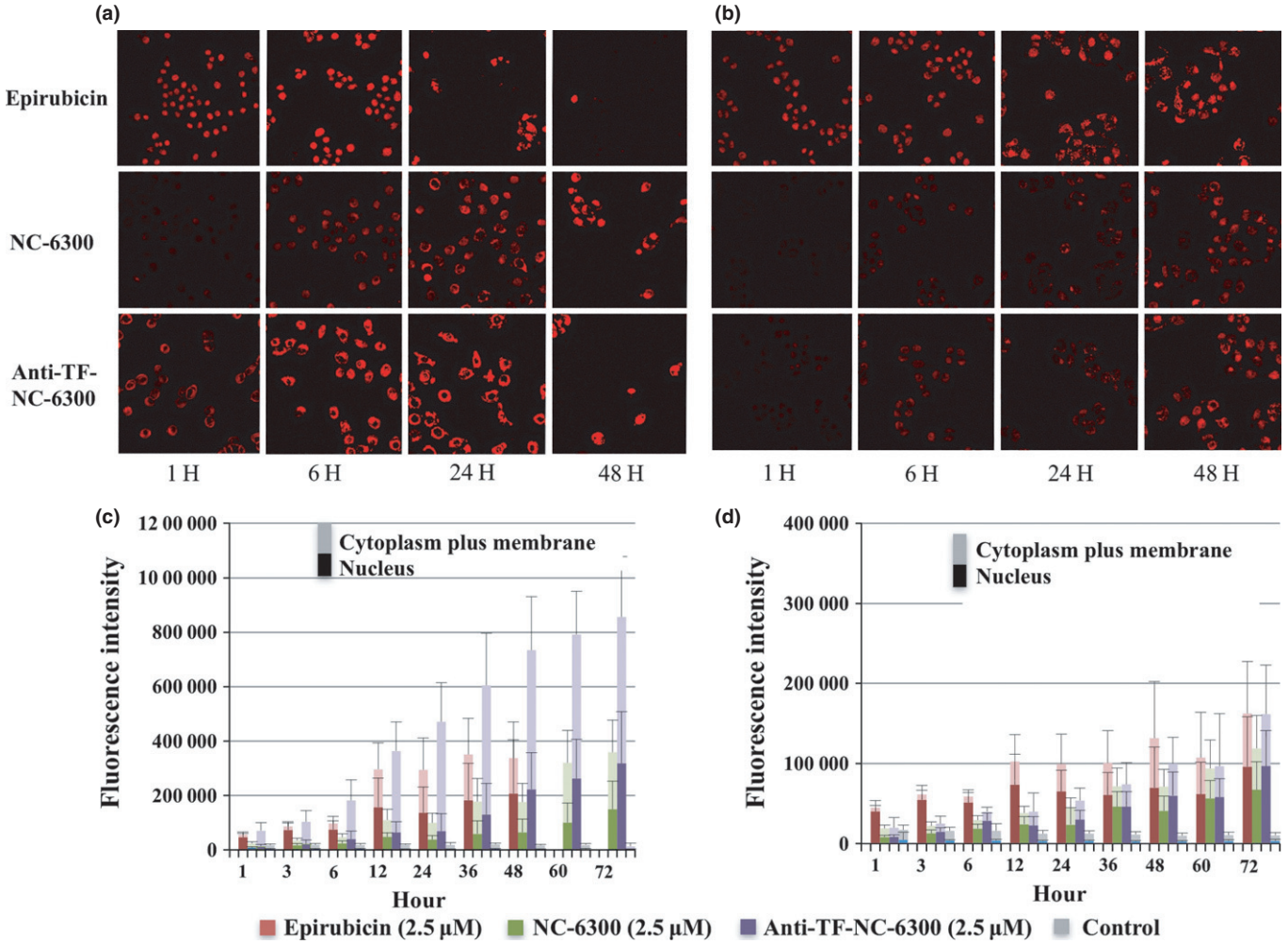

Fig. 2. Image analysis and quantification of the intracellular epirubicin concentration. BxPC3 cells (high tissue factor [TF] expression) (a), and SUIT2 cells (low TF expression) (b), were exposed to epirubicin, NC-6300, or anti-TF-NA-6300 at a concentration equivalent to 2.5 μM of epirubicin. The fluorescence signals of the intracellular epirubicin were quantified and represented as the mean total intensity in the cytoplasm plus membrane, or the nucleus of BxPC3 cells (c) and SUIT2 cells (d). Bars, SD.

In contrast, in the case of SUIT2 cells, epirubicin derived from anti-TF-NC-6300 showed almost the same behavior as that of NC-6300 (Fig. 2b). The mean value of the total fluorescence intensity of the epirubicin derived from anti-TF-NC-6300 in the cytoplasm plus membrane and in the nuclei per one BxPC3 cell was significantly higher than that derived from NC-6300 at 36 h ($P < 0.001$, $P < 0.001$, respectively) (Fig. 2c). However, no difference between the value for epirubicin derived from anti-TF-NC-6300 and from NC-6300 was observed in either the cytoplasm plus membrane or the nuclei of SUIT2 cells (low TF expression) ($P = 0.196$, $P = 0.935$, respectively) (Fig. 2d) (Table S1).

***In vitro* real-time growth-inhibition assay.** The growth curve of BxPC3 cells treated with anti-TF-NC-6300 reached a plateau at approximately 72 h and then dropped significantly thereafter. This pattern was distinctly different from that of the cells that were treated with NC-6300. The average cell index value at 120 h for the BxPC3 cells treated with anti-TF-NC-6300 was significantly lower than that of the cells treated with NC-6300 ($P < 0.001$) (Fig. 3a). However, the growth curve of the SUIT2 cells treated with anti-TF-NC-6300 showed a pattern similar to that of the cells treated with NC-6300. No difference in the cell index values at 120 h was observed between the SUIT2 cells treated with anti-TF-NC-6300 and those treated with NC-6300 ($P = 0.199$) (Fig. 3b).

***In vivo* antitumor effect of anti-TF-NC-6300 against human cancer xenograft models with high/low tissue factor expression.** The therapeutic effect of anti-TF-NC-6300 was significantly greater than that of NC-6300 and conventional epirubicin in both the 44As3 and the BxPC3 xenografts ($P = 0.003$ and $P < 0.001$ in 44As3, $P = 0.012$ and $P < 0.001$ in BxPC3, respectively) (Fig. 4a,c). In contrast, the effect of anti-TF-NC-6300 was almost equivalent to that of NC-6300 in the SUIT2 xenografts ($P = 0.794$) (Fig. 4e). The effect of NC-6300 was significantly greater than that of epirubicin in the 44As3 xenograft model ($P = 0.004$) (Fig. 4a). In the BxPC3 and SUIT2 xenografts, however, NC-6300 was not significantly superior to epirubicin ($P = 0.374$, $P = 0.065$, respectively) (Fig. 4c,e). The therapeutic effect of epirubicin was significantly greater than that of the control in the 44As3, BxPC3 and SUIT2 xenograft models ($P = 0.007$, $P = 0.007$ and $P < 0.001$, respectively) (Fig. 4a,c,e).

No severe body weight loss or toxicity-related death was observed in the anti-TF-NC-6300 and NC-6300 groups, but

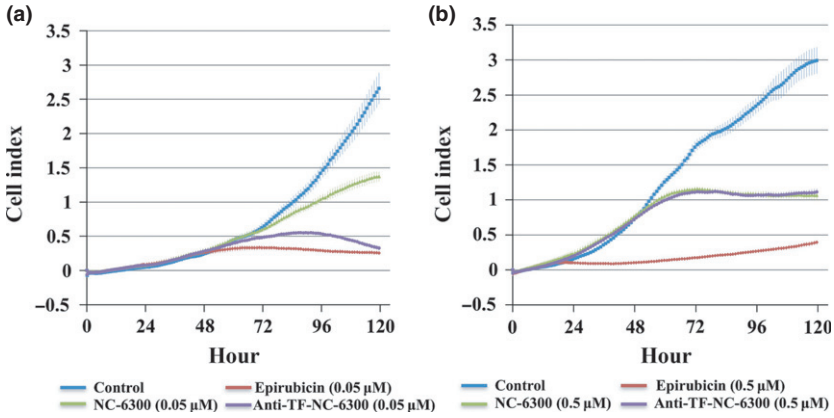

Fig. 3. In the *in vitro* assay, a real-time cell analysis was performed using the xCELLigence system to determine the effects of epirubicin, NC-6300 and anti-TF-NC-6300 on BxPC3 cells (a) or SUIT2 cells (b) (n = 5). Points, mean; bars, SD.

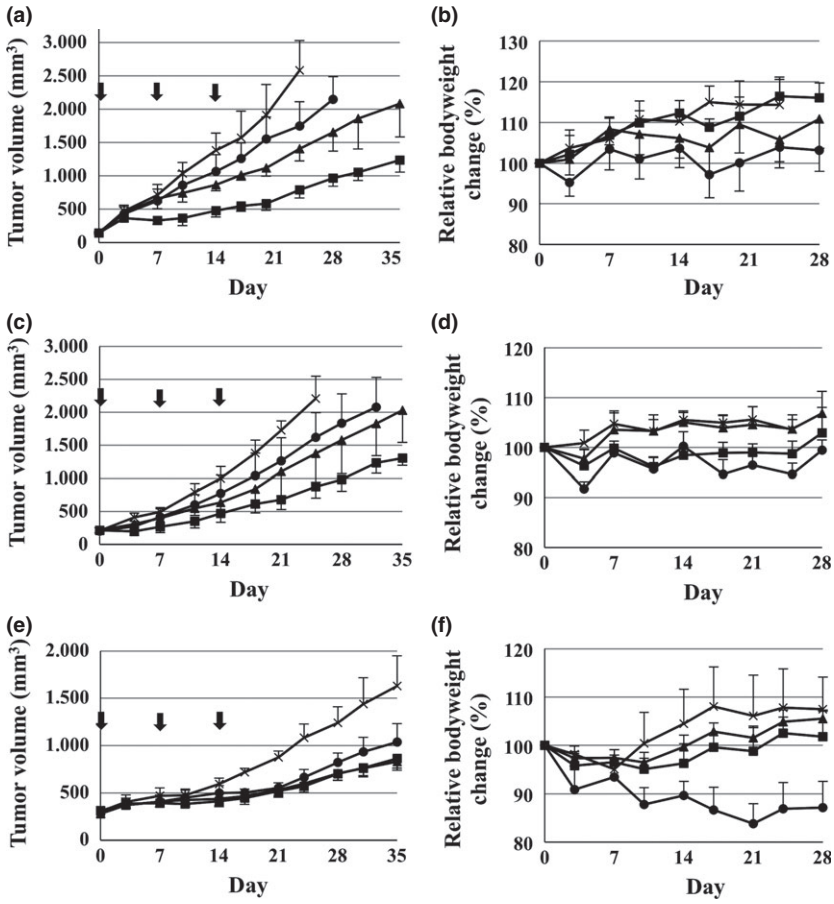

Fig. 4. *In vivo* antitumor activities and changes in relative body weight in mouse models bearing subcutaneous 44As3 (a, b), BxPC3 (c, d) and SUIT2 (e, f) xenografts. The treatments were administered on Days 0, 7 and 14 after the tumor volume reached a suitable size (Day 0) (n = 5). (×) Control, (●) epirubicin (10 mg/kg), (▲) NC-6300 (10 mg/kg) and (■) anti-TF-NC6300 (10 mg/kg). Points, mean; bars, SD; arrows, drug injections.

significant differences in body weight loss were observed between the epirubicin group and both groups of nanoparticles in all the cancer xenograft models (Fig. 4b,d,f).

Pharmacokinetic analysis. After the administration of anti-TF-NC-6300 or NC-6300, the highest tumor concentration of free epirubicin released from each micelle was observed from 6 to 24 h, with the drug concentration remaining high throughout the observation period in both the BxPC3 and SUIT2 tumors (Fig. 5a,b). The areas under the curve (AUC) of free epirubicin and total epirubicin derived from anti-TF-NC-6300 were higher than those derived from NC-6300 in BxPC3 tumor tissue. Furthermore, the same tendency was observed in the SUIT2 tumor tissue. The AUC ratio of free epirubicin released from anti-TF-NC-6300 relative to NC-6300 was 1.40 in the BxPC3 tumor tissue and 1.44 in the SUIT2 tumor tissue. Likewise, the AUC ratio of total epirubicin released from anti-TF-NC-6300 relative to NC-6300 was 1.48 in the BxPC3 tumor tissue, and 1.56 in the SUIT2 tumor tissue (Table 1). The AUC ratios of free epirubicin released from anti-TF-NC-6300 relative to NC-6300 were 1.04, 1.26 and 0.88 in the liver, kidney and plasma, respectively (Table 1).

Distribution of anti-TF-NC-6300 in tumor tissues with high/low tissue factor expression. The intratumor distribution of fluorescence-labeled anti-TF-NC-6300 in BxPC3 and SUIT2 tumor sections was evaluated using a fluorescence microscope. The fluorescence signals of anti-TF-NC-6300 were evenly

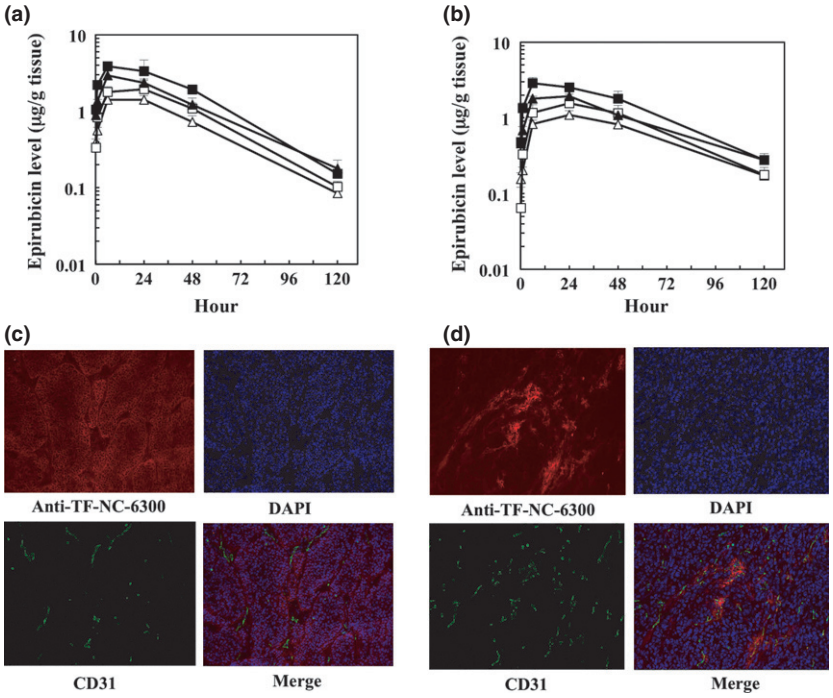

Fig. 5. The plasma and tissue concentration-time profiles of epirubicin after an administration of NC-6300 or anti-TF-NC-6300 to mice bearing subcutaneous BxPC3 (a) or SUIT2 (b) xenografts ($n = 3$) are shown. (□) Total epirubicin level from NC-6300 (10 mg/kg), (△) released epirubicin level from NC-6300 (10 mg/kg), (■) total epirubicin level from anti-TF-NC-6300 (10 mg/kg), (▲) released epirubicin level from anti-TF-NC-6300 (10 mg/kg). Points, mean; bars, SD. Distribution of Alexa Fluor®647-labeled anti-TF-NC-6300 in BxPC3 (c) or SUIT2 (d) xenografts after 24 h following i.v. injection (50 mg/kg).

Table 1. Areas under the curve (AUC) values of epirubicin in plasma and tissues after injection of anti-TF-NC-6300 at 10 mg/kg or NC-6300 at 10 mg/kg in mice bearing BxPC3 or SUIT2 xenografts

	AUC (mg/g tissue or mL × h)				Anti TF-NC-6300/NC-6300 AUC ratio	
	Anti TF-NC-6300		NC-6300			
	Released epirubicin	Total epirubicin	Released epirubicin	Total epirubicin	Released epirubicin	Total epirubicin
BxPC3						
Plasma	39.3	1645.2	49.3	1491.5	0.80	1.10
Liver	522.0	1179.0	502.2	1348.7	1.04	0.87
Kidney	258.9	479.0	205.9	337.6	1.26	1.42
Tumor	113.2	210.2	80.8	142.2	1.40	1.48
SUIT2						
Tumor	98.3	169.4	68.5	108.8	1.44	1.56

The AUC values of epirubicin were calculated using the linear trapezoidal rule.

distributed around each tumor cell even distant from the tumor blood vessels in the BxPC3 tumor sections at 24 h after drug administration, in which the intratumor concentration of micelle was reached the peak value (Fig. 5c). Nevertheless, in the SUIT2 tumor sections, the distribution of anti-TF-NC-6300 was limited around tumor blood vessels with high intensity levels (Fig. 5d).

Discussion

In refining the ADC process, the ACA that is added to the mAb is usually limited to three molecules so as to maintain the stability and performance of the antibody. Thus, the candidate agents are not ordinary ACA, but chemical compounds with extremely high toxicities, such as monomethyl auristatin E and DM1.[4] Otherwise, an unrealistic amount of ADC is needed if the mAbs are conjugated with an ordinary ACA.

Polymeric micelles possess a unique capacity to load an abundant ACA in their inner core. Actually, one anti-TF-NC-6300 molecule encapsulates approximately 600 molecules of epirubicin and contains four molecules of $F(ab')_2$ at the termini of PEG chains on the particle surface. Thus, the molecular ratio of epirubicin to $F(ab')_2$ is approximately 150:1. In the present study, the anti-TF-NC-6300 generated by this compounding ratio showed an enhanced antitumor effect, compared with NC-6300, in accordance with the degree of the TF expression levels in tumors. From the results of the *in vitro* assay, a significantly higher amount of epirubicin accumulated in the cytoplasm followed by its translocation into the nuclei of the cancer cells with a high TF expression in the case of anti-TF-NC-6300, compared with untargeted NC-6300. The difference in the antiproliferative effect between anti-TF-NC-6300 and NC-6300 against the cancer cells with TF high expression was clearly significant. In contrast, no significant difference was observed between anti-TF-NC-6300 and NC-6300 in cancer cells with low TF expression. Thus, the cytotoxicity of anti-TF NC-6300 appears to be dependent on the interaction of the anti-TF mAb on the micelle and the TF

antigen expressed on the cells. In contrast, free epirubicin internalized into the cells faster than the other micelles. However, this experiment was performed using an *in vitro* system. *In vivo*, free epirubicin should be cleared very quickly from the bloodstream and tumor tissue before exerting the antitumor activity.[13,14]

Unexpectedly, the AUC ratio of epirubicin released from anti-TF-NC-6300 relative to that released from NC-6300 in the BxPC3 tumor tissues (1.40) was similar to that in the SUIT2 tumor tissues (1.44). For the AUC ratio of total epirubicin, a similar tendency was also observed (Table 1). Plasma AUC of total epirubicin from anti-TF-NC-6300 was relatively higher than that of NC-6300 in mice bearing BxPC3 tumor (Table 1). There is a possibility that the change in size or surface electric charge of the nanoparticles by the antibody conjugation may cause the stability in blood stream, resulting in the increasing EPR effect in mice bearing both tumors. Namely, the tumor accumulation of both anti-TF-NC-6300 and NC-6300 may not have been caused by the anti-TF mAb, but may depend mainly on passive targeting based on the EPR effect. In contrast, the intratumor distributions of anti TF-NC-6300 were drastically changed by the degree of TF expression in tumor tissues. Anti-TF-NC-6300 could reach and be anchored in nests of cancer cells and showed the uniform distribution with a focus on tumor cell membranes in the tumor cells with TF high expression. Therefore, the significantly higher antitumor activity of anti-TF-NC-6300 might have been caused by the widespread intratumor distribution and the more efficient internalization in the tumor cells, compared with NC-6300. Several recent reports have suggested that tumor-targeting mAb and ligands increase the intracellular uptake of pegylated nanoparticles, such as immunoliposome, and do not enhance accumulation in solid tumors.[27–31]

For human cancers, the heterogeneity of tumor cells can limit the clinical development of ADC systems based on cell-specific antigens.[32–35] Moreover, conventional ADC depend on cleavage at the conjugation site via an intracellular biochemical (enzymatic) process after the uptake of the conjugate by the tumor cell.[36–39] In addition to such limiting characteristics of the cancer cells themselves, most human solid tumors, such as pancreatic cancer and gastric cancer, possess abundant stroma that hinders the distribution of macromolecules.[40–43] However, several reports (including ours) have confirmed that high TF expression levels occur not only on tumor cells, but also in cancer stroma (including tumor vascular endothelial cells) in humans.[44,45] The anti-TF antibody used in this study is a mAb against human TF, and it is not reactive to mouse TF expressed on host tumor vascular endothelial cells. Considering its possible clinical use, our anti-TF-NC-6300 may continue to exert a high antitumor activity despite the existence of the tumor stromal barrier, because anti-TF-NC-6300 was capable of suppressing tumor growth associated with damage to the tumor vessels and the death of cancer cells in humans.

Acknowledgments

This work was supported by the Funding Program for World-Leading Innovative R&D on Science and Technology (FIRST Program) (Y. Matsumura) and the National The authors thank Ms. M Nakayama for her secretarial assistance.

Disclosure Statement

The authors have no conflict of interest to declare.

References

1 Verma S, Miles D, Gianni L *et al.* Trastuzumab emtansine for HER2-positive advanced breast cancer. *N Engl J Med* 2012; **367**: 1783–91.
2 Younes A, Gopal AK, Smith SE *et al.* Results of a pivotal phase II study of brentuximab vedotin for patients with relapsed or refractory Hodgkin's lymphoma. *J Clin Oncol* 2012; **30**: 2183–9.
3 Pro B, Advani R, Brice P *et al.* Brentuximab vedotin (SGN-35) in patients with relapsed or refractory systemic anaplastic large-cell lymphoma: results of a phase II study. *J Clin Oncol* 2012; **30**: 2190–6.
4 Junutula JR, Raab H, Clark S *et al.* Site-specific conjugation of a cytotoxic drug to an antibody improves the therapeutic index. *Nat Biotechnol* 2008; **26**: 925–32.
5 Matsumura Y, Maeda H. A new concept for macromolecular therapeutics in cancer chemotherapy: mechanism of tumoritropic accumulation of proteins and the antitumor agent smancs. *Cancer Res* 1986; **46**: 6387–92.
6 Kataoka K, Kwon GS, Yokoyama M, Okano T, Sakurai Y. Block-copolymer micelles as vehicles for drug delivery. *J Control Release* 1993; **24**: 119–32.
7 Hamaguchi T, Matsumura Y, Suzuki M *et al.* NK105, a paclitaxel-incorporating micellar nanoparticle formulation, can extend in vivo antitumour activity and reduce the neurotoxicity of paclitaxel. *Br J Cancer* 2005; **92**: 1240–6.
8 Hamaguchi T, Kato K, Yasui H *et al.* A phase I and pharmacokinetic study of NK105, a paclitaxel-incorporating micellar nanoparticle formulation. *Br J Cancer* 2007; **97**: 170–6.
9 Kato K, Chin K, Yoshikawa T *et al.* Phase II study of NK105, a paclitaxel-incorporating micellar nanoparticle, for previously treated advanced or recurrent gastric cancer. *Invest New Drugs* 2012; **30**: 1621–7.
10 Nishiyama N, Okazaki S, Cabral H *et al.* Novel cisplatin-incorporated polymeric micelles can eradicate solid tumors in mice. *Cancer Res* 2003; **63**: 8977–83.
11 Uchino H, Matsumura Y, Negishi T *et al.* Cisplatin-incorporating polymeric micelles (NC-6004) can reduce nephrotoxicity and neurotoxicity of cisplatin in rats. *Br J Cancer* 2005; **93**: 678–87.
12 Plummer R, Wilson RH, Calvert H *et al.* A Phase I clinical study of cisplatin-incorporated polymeric micelles (NC-6004) in patients with solid tumours. *Br J Cancer* 2011; **104**: 593–8.
13 Harada M, Bobe I, Saito H *et al.* Improved anti-tumor activity of stabilized anthracycline polymeric micelle formulation, NC-6300. *Cancer Sci* 2011; **102**: 192–9.
14 Takahashi A, Yamamoto Y, Yasunaga M *et al.* NC-6300, an epirubicin-incorporating micelle, extends the antitumor effect and reduces the cardiotoxicity of epirubicin. *Cancer Sci* 2013; **104**: 920–5.
15 Yamamoto Y, Hyodo I, Takigahira M *et al.* Effect of combined treatment with the epirubicin-incorporating micelles (NC-6300) and 1,2-diaminocyclohexane platinum (II)-incorporating micelles (NC-4016) on a human gastric cancer model. *Int J Cancer* 2014; **135**: 214–23.
16 van den Berg YW, Osanto S, Reitsma PH, Versteeg HH. The relationship between tissue factor and cancer progression: insights from bench and bedside. *Blood* 2012; **119**: 924–32.
17 Colman RW, Marder VJ, Clowes AW, George JN, Goldhaber SZ. *Hemostasis and Thrombosis: Basic Principles and Clinical Practice*, 5th edn. Philadelphia, USA: Lippincott Williams & Wilkins, 2006.
18 Saito Y, Hashimoto Y, Kuroda J *et al.* The inhibition of pancreatic cancer invasion-metastasis cascade in both cellular signal and blood coagulation cascade of tissue factor by its neutralisation antibody. *Eur J Cancer* 2011; **47**: 2230–9.
19 Zhao J, Mi Y, Feng SS. Targeted co-delivery of docetaxel and siPlk1 by herceptin-conjugated vitamin E TPGS based immunomicelles. *Biomaterials* 2013; **34**: 3411–21.
20 Sawant RR, Jhaveri AM, Torchilin VP. Immunomicelles for advancing personalized therapy. *Adv Drug Deliv Rev* 2012; **64**: 1436–46.
21 Li W, Zhao H, Qian W *et al.* Chemotherapy for gastric cancer by finely tailoring anti-Her2 anchored dual targeting immunomicelles. *Biomaterials* 2012; **33**: 5349–62.
22 Yue J, Liu S, Wang R *et al.* Fluorescence-labeled immunomicelles: preparation, in vivo biodistribution, and ability to cross the blood-brain barrier. *Macromol Biosci* 2012; **12**: 1209–19.

23 Taylor RM, Sillerud LO. Paclitaxel-loaded iron platinum stealth immunomicelles are potent MRI imaging agents that prevent prostate cancer growth in a PSMA-dependent manner. *Int J Nanomedicine* 2012; **7**: 4341–52.
24 Liao C, Sun Q, Liang B, Shen J, Shuai X. Targeting EGFR-overexpressing tumor cells using Cetuximab-immunomicelles loaded with doxorubicin and superparamagnetic iron oxide. *Eur J Radiol* 2011; **80**: 699–705.
25 Torchilin VP, Lukyanov AN, Gao Z, Papahadjopoulos-Sternberg B. Immunomicelles: targeted pharmaceutical carriers for poorly soluble drugs. *Proc Natl Acad Sci USA* 2003; **100**: 6039–44.
26 Jin C, Qian N, Zhao W *et al.* Improved therapeutic effect of DOX-PLGA-PEG micelles decorated with bivalent fragment HAb18 F(ab')(2) for hepatocellular carcinoma. *Biomacromolecules* 2010; **11**: 2422–31.
27 Pirollo KF, Chang EH. Does a targeting ligand influence nanoparticle tumor localization or uptake? *Trends Biotechnol* 2008; **26**: 552–8.
28 Kirpotin DB, Drummond DC, Shao Y *et al.* Antibody targeting of long-circulating lipidic nanoparticles does not increase tumor localization but does increase internalization in animal models. *Cancer Res* 2006; **66**: 6732–40.
29 Mamot C, Drummond DC, Noble CO *et al.* Epidermal growth factor receptor-targeted immunoliposomes significantly enhance the efficacy of multiple anticancer drugs in vivo. *Cancer Res* 2005; **65**: 11631–8.
30 Bartlett DW, Su H, Hildebrandt IJ, Weber WA, Davis ME. Impact of tumor-specific targeting on the biodistribution and efficacy of siRNA nanoparticles measured by multimodality in vivo imaging. *Proc Natl Acad Sci USA* 2007; **104**: 15549–54.
31 Choi CH, Alabi CA, Webster P, Davis ME. Mechanism of active targeting in solid tumors with transferrin-containing gold nanoparticles. *Proc Natl Acad Sci USA* 2010; **107**: 1235–40.
32 Koenders PG, Peters WHM, Wobbes T, Beex LVAM, Nagengast FM, Benraad TJ. Epidermal growth-factor receptor levels are lower in carcinomatous than in normal colorectal tissue. *Br J Cancer* 1992; **65**: 189–92.
33 Messersmith W, Oppenheimer D, Peralba J *et al.* Assessment of epidermal growth factor receptor (EGFR) signaling in paired colorectal cancer and normal colon tissue samples using computer-aided immunohistochemical analysis. *Cancer Biol Ther* 2005; **4**: 1381–6.
34 Check Hayden E. Cancer complexity slows quest for cure. *Nature* 2008; **455**: 148.
35 Heng HH, Bremer SW, Stevens JB, Ye KJ, Liu G, Ye CJ. Genetic and epigenetic heterogeneity in cancer: a genome-centric perspective. *J Cell Physiol* 2009; **220**: 538–47.
36 Collins BE, Blixt O, Han S *et al.* High-affinity ligand probes of CD22 overcome the threshold set by cis ligands to allow for binding, endocytosis, and killing of B cells. *J Immunol* 2006; **177**: 2994–3003.
37 Schmidt MM, Thurber GM, Wittrup KD. Kinetics of anti-carcinoembryonic antigen antibody internalization: effects of affinity, bivalency, and stability. *Cancer Immunol Immunother* 2008; **57**: 1879–90.
38 Burke PJ, Senter PD, Meyer DW *et al.* Design, synthesis, and biological evaluation of antibody–drug conjugates comprised of potent camptothecin analogues. *Bioconjug Chem* 2009; **20**: 1242–50.
39 Coyne CP, Jones T, Pharr T. Synthesis of a covalent gemcitabine-(carbamate)-[anti-HER2/neu] immunochemotherapeutic and its cytotoxic anti-neoplastic activity against chemotherapeutic-resistant SKBr-3 mammary carcinoma. *Bioorg Med Chem* 2011; **19**: 67–76.
40 Dvorak HF. Tumors: wounds that do not heal. Similarities between tumor stroma generation and wound healing. *N Engl J Med* 1986; **315**: 1650–9.
41 Yasunaga M, Manabe S, Tarin D, Matsumura Y. Cancer-stroma targeting therapy by cytotoxic immunoconjugate bound to the collagen 4 network in the tumor tissue. *Bioconjug Chem* 2011; **22**: 1776–83.
42 Matsumura Y. Cancer stromal targeting (CAST) therapy. *Adv Drug Deliv Rev* 2012; **64**: 710–9.
43 Hisada Y, Yasunaga M, Hanaoka S *et al.* Discovery of an uncovered region in fibrin clots and its clinical significance. *Sci Rep* 2013; **3**: 2604.
44 Kothari H, Pendurthi UR, Rao LV. Analysis of tissue factor expression in various cell model systems: cryptic vs. active. *J Thromb Haemost* 2013; **11**: 1353–63.
45 Song HB, Park KD, Kim JH, Kim DH, Yu YS, Kim JH. Tissue factor regulates tumor angiogenesis of retinoblastoma via the extracellular signal-regulated kinase pathway. *Oncol Rep* 2012; **28**: 2057–62.

Supporting Information

Additional supporting information may be found in the online version of this article:

Table S1. The comparison of the mean value of the intracellular total fluorescence intensity of the epirubicin derived from anti-TF-NC-6300 and NC-6300.